Certified Localized Weil Positivity Through Support 0.72: Multiband Schur Complements and a Complete Stieltjes Hierarchy

Lluis Eriksson
Independent Researcher
lluiseriksson@gmail.com

August 2026

Abstract

Suzuki's localized Weil form is represented by a lower-bounded self-adjoint operator A_a on $L^2(-a,a)$; nonnegativity for every $a>0$ is equivalent to the Riemann hypothesis, while positivity at one fixed support is an unconditional and strictly weaker problem. We give a source-level interval certificate for the fixed-support inequality

$$A_{0.72} \succeq 5.890 \times 10^{-17}\mathrm{I} > 0.$$

Nested-core monotonicity then gives the same scalar lower bound for every $0 < a \le 0.72$. The proof is not a positive Ritz computation. It decomposes the exact prime-power translation graph through $n = 4$ into thirteen intervals, retains endpoint and singular directions as interval Gram matrices, and bounds the infinite complement by a mode-sensitive Schur estimate. The decisive split isolates degrees $12,\dots,23$, followed by $[24,176)$ and $[176,\infty)$; both parity Schur matrices have 78 certified positive directions and no unresolved direction at 512-bit Arb precision. An independent shadow implementation, importing neither the project nor python-flint, reconstructs the prime-power graph and parity maps and reassembles the exported Schur balls with high-precision arithmetic; it is a wiring audit rather than a substitute for the Arb proof.

Two analytic results explain why this certificate scales beyond a single matrix. First, the boundary potential $-\frac{1}{2}\log(1-x^2)$ has an exact Gauss–Stieltjes hierarchy whose finite approximants increase by explicit Schur squares and whose Markov remainder is a continuous square. At every fixed support this is a complete terminating strict-positivity hierarchy. Second, harmonic complement denominators admit a $(1+\varepsilon)$ Loewner Schur majorant with only $O_\varepsilon(\log\log M)$ bands through degree M. The ingredients of Gaussian quadrature and operator antitonicity are classical; the contribution is their source-faithful integration with the arithmetic translations into a rigorous coercivity certificate. This is a bounded-support theorem, not a proof of the Riemann hypothesis.

Keywords. Weil quadratic form; Riemann zeta function; localized operator; interval arithmetic; Schur complement; Gauss quadrature; Stieltjes function; Legendre expansion.

1 Statement, context, and claim boundary

Let Q_W denote the global Weil quadratic form in Suzuki's additive logarithmic convention, and let Q_W^a be its closed restriction to functions supported in $(-a,a)$. Suzuki constructs the representing self-adjoint operator A_a on $L^2(-a,a)$ and identifies

$$\lambda_a := \min \operatorname{spec}(A_a) = \inf_{0 \ne v \in C_c^\infty(-a,a)} \frac{Q_W(v)}{\|v\|_2^2}. \tag{1}$$

The form is continuous in a, positive for sufficiently small support, and the global Weil criterion asks for nonnegativity at every support [5, 1, 2]. A finite-support lower bound is therefore meaningful but cannot by itself decide the Riemann hypothesis.

Our main result is the following computer-assisted theorem. All finite quantities in its proof are outward-rounded real balls; floating eigenvectors are used only to propose a congruence and never to decide a sign.

Theorem 1.1 (localized coercivity)**.** *In Suzuki's normalization of the global localized Weil form,*

$$\boxed{A_{0.72} \succeq 5.890 \times 10^{-17}\mathrm{I} > 0.} \tag{2}$$

Consequently, for every $0 < a \le 0.72$*,*

$$\lambda_a \ge 5.890 \times 10^{-17}. \tag{3}$$

The endpoint 0.72 is not claimed optimal. Among the primary sources we located, the previous explicit rigorous localized radius is Yoshida's $a = (\log 2)/2$ result, reproduced and discussed by Bombieri [1, 2]. Connes–Consani report larger numerical tests, and Kim et al. give a finite-element realization of Suzuki's operator, but positive Ritz values are upper bounds and do not certify coercivity [3, 6]. The present endpoint crosses the active prime-power channels $n = 2, 3, 4$, since $4 < e^{1.44} < 5$.

Remark 1.2 (not the semilocal scaling Hamiltonian)**.** *The operator in theorem 1.1 is only the self-adjoint representative of Suzuki's closed global localized form. We do not identify it with a semilocal Connes–Consani operator: that formulation has a different sign convention, two moment constraints, multiplicative convolution, and a globally normalized principal value. No operator ordering between different a is asserted, because the operators act on different Hilbert spaces.*

2 Source normalization and nested-core monotonicity

We record the normalization because a wrong polar Gram changes the odd sector. Put

$$\widehat{v}(z) = \int_{\mathbb{R}} v(x) e^{izx}\,\mathrm{d}x, \qquad \widetilde{v}(x) = \overline{v(-x)}, \qquad f = v * \widetilde{v}.$$

Then $f(0) = \|v\|_2^2$. In the direct explicit-formula representation the polar contribution is

$$V_+\overline{V_-} + V_-\overline{V_+} = 2\,\mathrm{Re}(V_+\overline{V_-}), \qquad V_\pm = \int v(x) e^{\pm x/2}\,\mathrm{d}x, \tag{4}$$

not $|V_+|^2 + |V_-|^2$. The scalar term is $-(\log(4\pi) + \gamma)\|v\|_2^2$, while the arithmetic part is

$$-\sum_{n\ge 2} \frac{\Lambda(n)}{\sqrt{n}} \big[f(\log n) + f(-\log n)\big]. \tag{5}$$

For support $[-a, a]$ the unsampled archimedean tail contributes the exact $-2\,\mathrm{atanh}(e^{-2a}) f(0)$ inside the archimedean integral. These conventions agree with Suzuki's global form and are independently exercised by the source code.

Proposition 2.1 (nested-core monotonicity)**.** *If $0 < a' \le a$, then $\lambda_{a'} \ge \lambda_a$. In particular, $A_a \succeq c\mathrm{I}$ implies $\lambda_{a'} \ge c$ for all $a' \le a$.*

Proof. Extension by zero embeds $C_c^\infty(-a', a')$ into $C_c^\infty(-a, a)$ and preserves both the L^2 norm and the value of the same global functional Q_W. The admissible Rayleigh quotients for the smaller interval are therefore a subset of those for the larger interval. Apply (1). This compares scalar infima, not operators on different spaces. □

Thus the numerical-analytic burden is entirely at the largest endpoint. Continuity additionally implies that, if the Riemann hypothesis is false, the negative set of λ_a is an upper open interval. A zero plateau is not excluded, so no simple or transverse crossing is claimed.

3 The scale-free dominant operator

After scaling $(-a, a)$ to $(-1, 1)$, the dominant archimedean form is

$$\mathcal{L} = A_2 + V, \qquad (A_2 w)(x) = \frac{1}{2}\int_{-1}^{1} \frac{w(x) - w(y)}{|x - y|}\,\mathrm{d}y, \qquad V(x) = -\frac{1}{2}\log(1 - x^2). \tag{6}$$

The regional logarithmic Laplacian is exactly diagonal in the Legendre basis:

$$A_2 P_n = H_n P_n, \qquad H_n = \sum_{k=1}^{n} \frac{1}{k}, \quad H_0 = 0, \tag{7}$$

as established in the recent analysis of the interval logarithmic Laplacian [7]. The remaining bounded block contains the scalar, smooth, and finitely many translation terms. For $a = 0.72$ its active arithmetic displacements are $\log 2/a$, $\log 3/a$, and $\log 4/a$; the last weight is $-\Lambda(4)/2 = -\log 2/2$, not $-\log 4/2$.

Cutting the interval at all translation endpoints gives thirteen subintervals. Their pointwise translation graph has components of sizes seven, four, and two. Local normalized Legendre coordinates turn every exact translation between equal-length intervals into an identity block. The finite source keeps twelve local degrees on each interval. Reflection reduces the resulting 156-dimensional source into two 78×78 parity blocks.

Proposition 3.1 (exact third-window partition). *Suppose*

$$\log 2 < a < \frac{1}{2}\log\frac{9}{2}, \qquad h_2 = \frac{\log 2}{a}, \qquad h_3 = \frac{\log 3}{a}.$$

In the scaled interval $[-1, 1]$*, the ordered cut points are*

$$\begin{gathered}-1,\ 1-2h_2,\ -1+2h_2-h_3,\ 1-h_3,\ -1-h_2+h_3,\\ 1-3h_2+h_3,\ -1+h_2,\ 1-h_2,\ -1+3h_2-h_3,\\ 1+h_2-h_3,\ -1+h_3,\ 1-2h_2+h_3,\ -1+2h_2,\ 1.\end{gathered}$$

Numbering the resulting intervals $0, \ldots, 12$*, translations by* h_2*,* h_3*, and* $2h_2$ *pair respectively*

$$\begin{aligned}&(0,6),(1,7),(2,8),(3,9),(4,10),(5,11),(6,12),\\ &(0,10),(1,11),(2,12), \qquad (0,12).\end{aligned}$$

Hence the translation graph components are

$$\{0,2,4,6,8,10,12\}, \qquad \{1,5,7,11\}, \qquad \{3,9\}.$$

All intervals in one component have the same length.

Proof. The endpoints are the orbit of $\{-1, 1\}$ required to make the three translations map whole cells to whole cells. Their consecutive differences repeat the three values

$$2(1-h_2), \qquad 4h_2-h_3-2, \qquad 2h_3-h_2-2.$$

The first is positive because $a > \log 2$; the third is positive exactly when $2a < \log(9/2)$; and the middle is then positive as well because $\log(9/2) < \log(16/3)$. This proves the ordering. Direct subtraction of paired endpoints gives the three edge lists. Graph connectivity gives the components; their interval lengths are respectively the first, second, and third displayed values. For $a = 0.72$, the window inequalities hold. $\square$

Thus the arithmetic term in the local orthonormal Legendre basis is an exact weighted graph matrix: every listed n-edge is $-\Lambda(n)/\sqrt{n}$ times an identity block. In particular, the sole $n = 4$ edge has coefficient $-\log 2/2$. This algebraic partition, rather than a sampled quadrature grid, is what the interval source generator encloses.

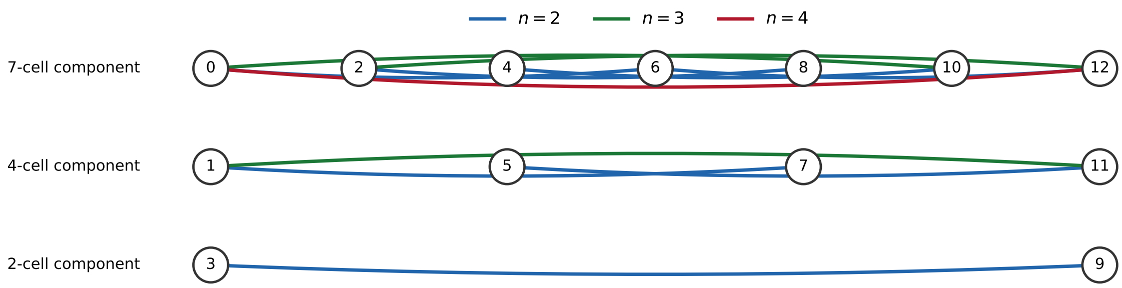

Figure 1: Exact translation graph of the thirteen interval cells. Each row is one pointwise connected component; edge colors record the prime-power channel. The layout is schematic, while the vertex labels and edge set are the exact data used by the source generator.

4 An exact Gauss–Stieltjes hierarchy

The positive boundary potential can be retained rather than paid as a norm. Set $y = x^2$. The elementary Stieltjes identity

$$V(x) = \frac{1}{2}\int_0^1 \frac{y}{1-ty}\,\mathrm{d}t \tag{8}$$

leads to a hierarchy that we now make explicit. Let $(t_j, w_j)_{j=1}^m$ be the m-node Gauss–Legendre rule on $[0, 1]$ and define

$$R_m(x) = \frac{1}{2}\sum_{j=1}^{m} w_j \frac{x^2}{1-t_j x^2}. \tag{9}$$

Theorem 4.1 (exact Stieltjes hierarchy)**.** *For $0 < |x| < 1$,*

$$0 < R_1(x) < R_2(x) < \cdots < V(x), \tag{10}$$
$$R_m(1) = H_m, \tag{11}$$

where the endpoint value means the finite rational limit. If $p_m(t) = P_m(2t-1)$ and $q_m(y) = y^m p_m(1/y)$, then

$$V(x) - R_m(x) = \frac{1}{2}\int_0^1 \left(\frac{x^{2m+1}p_m(t)}{q_m(x^2)\sqrt{1-tx^2}}\right)^2 \mathrm{d}t. \tag{12}$$

Let J_m be the shifted-Legendre Jacobi matrix, with diagonal $1/2$ and links

$$a_k = \frac{k}{2\sqrt{(2k-1)(2k+1)}}.$$

Then

$$R_m(x) = \frac{x^2}{2}e_0^T(\mathrm{I} - x^2 J_m)^{-1}e_0, \tag{13}$$

and, writing $A_m = \mathrm{I} - x^2 J_m$ and

$$s_m = 1 - \frac{x^2}{2} - x^4 a_m^2 e_{m-1}^T A_m^{-1} e_{m-1} > 0,$$

one has the positive increment

$$R_{m+1}(x) - R_m(x) = \frac{x^6 a_m^2}{2s_m}\left(e_{m-1}^T A_m^{-1} e_0\right)^2. \tag{14}$$

Proof. For $z \notin [0,1]$, Gaussian exactness applied to $(p_m(z)^2 - p_m(t)^2)/(z-t)$ gives the classical Markov identity

$$p_m(z)^2\left(\int_0^1 \frac{\mathrm{d}t}{z-t} - \sum_j \frac{w_j}{z-t_j}\right) = \int_0^1 \frac{p_m(t)^2}{z-t}\,\mathrm{d}t.$$

Put $z = x^{-2}$ and rearrange to obtain (12). The endpoint identity follows by applying Gaussian exactness to $(1-p_m(t))/(1-t)$ and the standard Legendre integral $\int_{-1}^1 (1-P_m(s))/(1-s)\,\mathrm{d}s = 2H_m$. The spectral theorem for Gaussian quadrature gives (13). Since J_m is the leading principal block of J_{m+1} and its spectrum is inside $(0,1)$, block inversion gives (14). Positivity of the Schur complement proves strict nesting. □

The Gauss–Legendre/Padé theory itself is classical [8, 9]. The point here is that its positive remainder and positive increments match exactly the boundary potential of the localized Weil operator.

Corollary 4.2 (fixed-support completeness)**.** *Let $L_{a,m} = A_2 + R_m + B_a$ and $L_a = A_2 + V + B_a$, where B_a is the bounded scalar, smooth, and arithmetic block at fixed support. Then, for every fixed eigenvalue index k,*

$$\lambda_k(L_{a,m}) \nearrow \lambda_k(L_a).$$

In particular, $L_a \succ 0$ if and only if $L_{a,m} \succ 0$ for some finite m.

Proof. The forms increase pointwise by theorem 4.1. The harmonic diagonal $H_n \to \infty$ and a bounded perturbation give compact resolvent. Monotone convergence of closed forms and the min–max principle give eigenvalue convergence [11, 12]. Strict positivity of L_a leaves a positive first-eigenvalue margin reached at finite m; the converse is the pointwise operator order. □

This hierarchy does not settle a semidefinite zero-ground case and offers no support-uniform bound as $a \to \infty$; those qualifications prevent any RH conclusion.

5 Mode-sensitive Schur complements

We isolate the operator inequality that turns rigorous component Grams into a full infinite-dimensional certificate.

Theorem 5.1 (degree-resolved Schur majorant)**.** *Let $\mathcal{H} = \mathcal{H}_0 \oplus \mathcal{H}_1$ and*

$$T = \begin{pmatrix} A & B \\ B^* & D \end{pmatrix} = T^*.$$

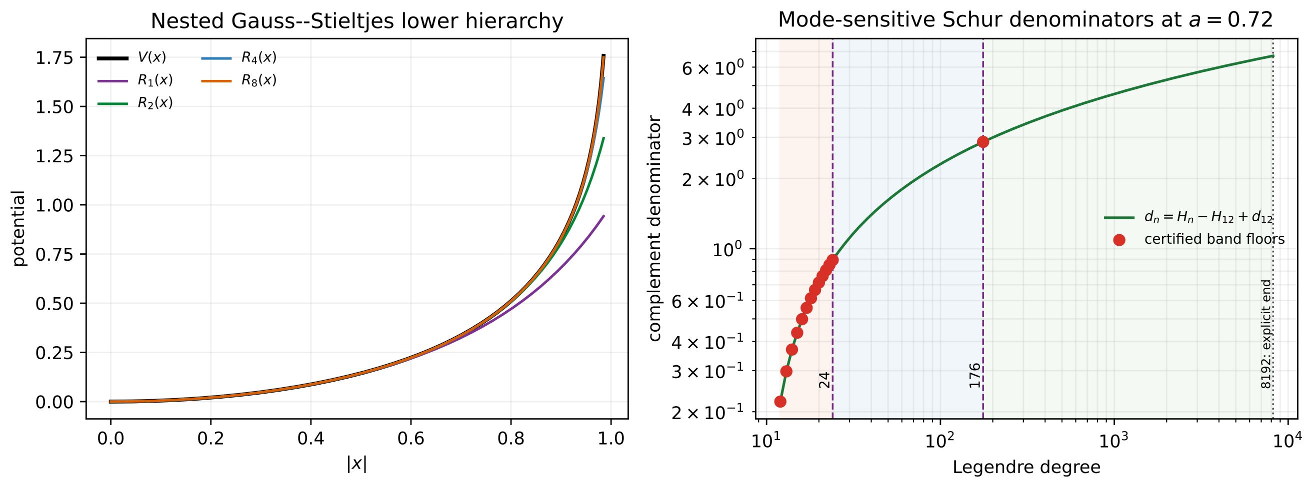

Figure 2: Left: exact nested lower approximants to the logarithmic boundary potential. Right: harmonic denominators and the three registered floors in the support-0.72 Schur certificate. The plots illustrate proved formulas; no sampled curve decides a sign.

Suppose $\{P_n\}_{n\geq N}$ *are mutually orthogonal projections summing to the identity on* $\mathcal{H}_1$ *and*

$$D \succeq \sum_{n\geq N} d_n P_n, \qquad d_n > 0. \tag{15}$$

Then

$$BD^{-1}B^* \preceq R_* := \sum_{n\geq N} \frac{(BP_n)(BP_n)^*}{d_n}. \tag{16}$$

For consecutive bands $I_j = [m_j, m_{j+1})$*, define*

$$R_{\mathcal{P}} = \sum_j \frac{1}{d_{m_j}} \sum_{n\in I_j} (BP_n)(BP_n)^*.$$

If d_n *is increasing and* $d_n \leq (1+\varepsilon)d_{m_j}$ *on* I_j*, then*

$$R_* \preceq R_{\mathcal{P}} \preceq (1+\varepsilon)R_*. \tag{17}$$

If $d_n = H_n + c > 0$*, a greedy partition through degree* M *uses at most*

$$1 + \left\lceil \frac{\log(d_{M-1}/d_N)}{\log(1+\varepsilon)} \right\rceil = O_\varepsilon(\log\log M) \tag{18}$$

bands.

Proof. Inverse antitonicity on positive operators applied to (15) gives $D^{-1} \preceq \sum d_n^{-1}P_n$, hence (16). On a band, $d_n^{-1} \leq d_{m_j}^{-1} \leq (1+\varepsilon)d_n^{-1}$; multiply by each positive Gram and sum. Greedy band starts make successive denominators grow geometrically, and $H_M \sim \log M$ gives (18). □

Lemma 5.2 (interval congruence judge)**.** *Let* $S = S^*$ *on* $\mathbb{R}^r$*, and let* X *be a real square matrix. If interval arithmetic proves*

$$X^TX \preceq u\mathrm{I}, \qquad X^TSX \succeq g\mathrm{I}, \qquad 0 < g, \quad u < \infty,$$

then X *is invertible as soon as a positive lower bound for* X^TX *is also certified, and*

$$S \succeq \frac{g}{u}\mathrm{I}. \tag{19}$$

It is enough to establish both matrix inequalities by outward-rounded Gershgorin bounds.

Proof. For $z = Xy$, one has $y^TX^TSXy \geq g\|y\|^2$ and $\|z\|^2 = y^TX^TXy \leq u\|y\|^2$. The positive lower Gram bound makes X onto, so (19) holds for every z. □

Lemma 5.3 (full block coercivity)**.** *For the block operator in theorem 5.1, suppose*

$$D \succeq d\mathrm{I}, \qquad A - BD^{-1}B^* \succeq s\mathrm{I}, \qquad \|B\| \le b, \qquad d, s > 0.$$

Then

$$T \succeq \left(\frac{(1 + b/d)^2}{s} + \frac{1}{d} \right)^{-1} \mathrm{I}. \tag{20}$$

If $BB^* \preceq G$, the computable substitution $b \le \sqrt{\operatorname{Tr} G}$ is valid.

Proof. Put $w = v + D^{-1}B^*u$. Block Gaussian elimination gives

$$\langle (u, v), T(u, v) \rangle \ge s\|u\|^2 + d\|w\|^2.$$

Moreover $\|(u, v)\| \le (1 + b/d)\|u\| + \|w\|$. Weighted Cauchy–Schwarz proves (20). The trace bound follows from $\|B\|^2 = \|BB^*\| \le \operatorname{Tr} G$. □

This theorem does not require D to preserve the individual degree spaces. That point is essential: (15) is a form inequality, and inverse antitonicity supplies the comparison without an invariance assumption. The Schur–Feshbach principle then says that positivity of $A - R_{\mathcal{P}}$ suffices for positivity of T. The two lemmas state exactly how an interval sign on that finite Schur matrix is transported back to a scalar lower bound for the full operator.

6 The support-0.72 certificate

6.1 Frozen architecture

We now list every load-bearing parameter. The finite source uses the exact thirteen-interval graph and twelve local Legendre modes per interval. The complement starts at local degree 12, the explicitly enclosed tail ends at 8192, the analytic smooth expansion has order 47, and all proof balls use 512-bit precision. The successful partition is

$$[12, 13), \ldots, [23, 24), \qquad [24, 176), \qquad [176, \infty). \tag{21}$$

The first and last finite-band denominator bounds, together with the far-tail bound, are

$$d_{12} \ge 0.2209732158977950, \quad d_{24} \ge 0.8937207154406235, \quad d_{176} \ge 2.868300416471574. \tag{22}$$

The twelve degreewise bounds increase monotonically between d_{12} and $d_{23} \ge 0.8520540487739568$.

proof item	frozen value
support and active prime powers	$a = 0.72$; $n = 2, 3, 4$
translation components	$7 + 4 + 2 = 13$ intervals
local source degrees	$0, \ldots, 11$ on every interval
source/parity dimensions	$156 = 78 + 78$
explicit complement range	$12 \le n < 8192$
smooth/self remainder endpoints	47 and 32768
pointwise subdivisions	1024
ball precision	512 bits

6.2 Fail-closed finite reduction

The aggregate $[12, 176)$ coupling Gram is generated independently from twelve nonzero degreewise Grams on $[12, 24)$. The residual $[24, 176)$ Gram is formed as an Arb interval subtraction, not by subtracting floating midpoints. Endpoint flux, adjacent singular, other-tail, and directional self-tail contributions enter as Grams before the final Schur subtraction.

For each parity π, the verifier performs the following fixed sequence.

1. It encloses the source matrix A_π, the aggregate Gram $G_\pi^{[12,176)}$, the independently generated degree Grams $G_\pi^{[m,m+1)}$ for $12 \le m < 24$, and the far-tail Gram.
2. It forms $G_\pi^{[24,176)} = G_\pi^{[12,176)} - \sum_{m=12}^{23} G_\pi^{[m,m+1)}$ as an Arb matrix subtraction, retaining every entry radius.
3. It subtracts the fourteen band corrections using the registered degreewise lower endpoints and the far-tail endpoint in (22), together with the endpoint, singular, smooth, and self-tail budgets, to obtain one interval Schur matrix S_π.
4. A floating midpoint eigensystem proposes X_π. The sign decision is then repeated entirely in Arb: positive lower Gram for $X_\pi^T X_\pi$, strict Gershgorin positivity for $X_\pi^T S_\pi X_\pi$, and the transport in theorem 5.2.

5. Any nonpositive denominator, noninvertible Gram, overlapping Gershgorin disc, metadata mismatch, or unresolved coercive lower endpoint aborts rather than returning a sign.

Table 1: Final interval adjudication at $a = 0.72$.

sector	negative	positive	unresolved	Schur lower
even	0	78	0	1.550×10^{-14}
odd	0	78	0	4.368×10^{-11}

6.3 Return to the full Hilbert space

For each parity, a floating midpoint eigenbasis proposes a change of basis. The verifier then proves with Arb that its Gram is positive, so the change is invertible, and that the congruent Schur interval is strictly Gershgorin positive. Finally, an interval upper bound on the squared norm of the change of basis transports the lower bound to the original coordinates. The block reconstruction, including the complement and coupling norm, gives respectively 5.890×10^{-17} and 1.652×10^{-13} in the even and odd sectors. The smaller number proves (2) by Lemma 5.3; this last step charges the norm of the source–complement coupling and is not an inference from the finite Schur eigenvalue alone.

Remark 6.1 (why a finite eigenvalue is insufficient)**.** *Rayleigh–Ritz gives upper bounds on the lowest eigenvalue. The proof instead certifies a lower bound on the full complement, encloses the source-to-tail coupling, and proves positivity of the resulting interval Schur matrices. Every omitted infinite direction is charged before the sign is decided.*

7 Reproducibility and falsification gates

The proof source starts from repository commit `3d997887ccf4e056607c4488a708181db1d507ef`; the release includes the complete source snapshot and the audited accumulator patches that produced format version 3. Two interval proof objects and the final JSON record have the registered names and SHA-256 digests

- `theta-schur-a072-d12-p47-tail8192-v3.npz`:
  `fab69bc8fa1d21ac0d3faca85d317ec5655fd991e7af29329329be4e5f8c1ebb`;
- `theta-near-band-a072-d12-to24-by-degree-p512-v3.npz`:
  `9119dbd4bad1a3c0de406445bbcb537e7c6d10fc6010f7a9d90ea79ae561751c`;
- `theta-schur-a072-multiband-to24-by-degree-v3.json`:
  `63b0dd91dab9fe7a00b734644c7a0400c2240a51cc25e6dde42751208dfc4f08`.

The first artifact is a deterministic outward upgrade of the allowlisted pre-refactor aggregate: its intrinsic radii are rounded up, one centre ulp is added, and the exact smooth remainder is rounded up. An independent corrected replay has identical component midpoints and strictly nonzero aggregate Grams. The second artifact is the directly regenerated degreewise $[12, 24)$ family; the third is the theorem record. Format version 3 records the corrected list accumulation and centred-binary64 export, and rejects both earlier artifact schemas. Metadata checks include support, degrees, partition, smooth order, and precision. The release wrapper additionally checks all expected keys, 78×78 shapes, numeric finiteness, nonnegative radii, the JSON theorem schema, and the three byte hashes before accepting a replay. Format version 3 also widens every stored radius by one ulp of its binary64 centre, so the cache encloses both the Arb ball and the centre-conversion displacement. A mismatch fails closed.

The proof is falsifiable at several levels: a nonpositive complement denominator aborts; a nonpositive change-of-basis Gram aborts; any overlapping Gershgorin ball is unresolved rather than rounded positive; any hash mismatch rejects the frozen record; and parity reconstruction is checked independently against the unreduced source. The release includes the allowlisted predecessor, the conservative upgrader, the fresh provenance replay, and their comparison record; these are proof objects, not untracked assumptions.

The frozen environment is Python 3.12.6, python-flint 0.9.0, NumPy 2.5.1, SciPy 1.18.0, and mpmath 1.3.0. The heavy component generators were run on a Colab Pro+ CPU runtime at 512-bit Arb precision; the aggregate replay took approximately 80 minutes on that runtime. The final verifier takes about two seconds and the independent shadow audit about nine seconds on the stated desktop environment. The public source is the linked repository commit. The exact archive accompanying this manuscript is `Certified_Localized_Weil_Positivity_Through_Support_0_72_Reproducibility.zip`, with SHA-256

`b5ace98f5ac8951c3939ee85c4c34563`
`668861b0c23ca3751e7e4d5b17eb2645`.

Its README prints both replay commands; the terminal acceptance command is

`python repro/verify_release.py repro`.

8 Relation to previous work and limitations

Yoshida and Bombieri established the localized variational setting and a first explicit support result [1, 2]. Connes–Consani and Connes–Consani–Moscovici developed operator and spectral-triple realizations of Weil positivity [3, 4]. Suzuki's screw-function framework supplies the precise self-adjoint operator certified here [5]. Kim et al. numerically instantiate that operator and show the severe resolution problem in its lowest branch [6].

Classical inputs are not novelty claims: Gaussian quadrature, Padé/Markov remainders, Jacobi resolvents, operator inverse antitonicity, Schur complements, and monotone convergence of forms are standard [8, 9, 10, 11, 12]. The contributions are:

1. a source-faithful coercivity certificate for the complete operator at support 0.72, rather than a positive compression;
2. a mode-sensitive arithmetic Schur construction that retains the exact prime-power graph through $n = 4$ and closes both parity sectors;
3. the specialization of the exact Stieltjes hierarchy to Suzuki's boundary potential, including a terminating strict-positivity hierarchy at fixed support; and
4. a multiband theorem showing that harmonic inverse tails can be controlled with doubly logarithmic storage.

The result has sharp logical limits. It does not prove positivity beyond 0.72, does not establish support-uniform constants, does not prove RH, does not identify zeta zeros as eigenvalues of A_a, and does not turn numerical agreement with known zeros into a premise. Further isolated endpoints would extend the unconditional interval but would not by themselves solve the uniform-support problem. A global advance needs a source-side stratification whose finite Schur sign remains controlled as new prime powers enter.

A Source-to-Gram specification

This appendix makes the software boundary explicit. It is normative for the certificate: every term subtracted from the finite source is listed with its mathematical sign and the routine that encloses it.

A.1 Finite source

Let I_r be the thirteen intervals of Proposition 3.1 and let e_{rj} be the normalized local Legendre mode of degree $j < 12$ on I_r. Write $\ell_r = |I_r|$. The scale-free diagonal-block entries used by the generator are

$$D^{(r)}_{jk} = \begin{cases} H_j + 1 + \sum_{m=1}^{j} \dfrac{1}{m(2m-1)(2m+1)} - \log 2 - \log(\ell_r/2), & j = k, \\ \dfrac{\sqrt{(2j+1)(2k+1)}}{|j-k|(j+k+1)}, & j \neq k,\ j+k \text{ even}, \\ 0, & j+k \text{ odd}. \end{cases} \tag{23}$$

Cross-interval entries are exact Legendre moments of the logarithmic kernel. The smooth archimedean remainder is expanded through power 47. If up_2 denotes the two successive outward binary64 roundings used at generation and adjudication, its charged scalar is

$$r_{\mathrm{sm}} := \mathrm{up}_2\left(2a\left[\frac{2}{3}\frac{(2a/3)^{48}}{1-2a/3} + \frac{2a^{48}/48!}{1-a^2/(49\cdot 50)}\right]\right) = 9.2437306756331 \times 10^{-16}. \tag{24}$$

This is an unsigned Schur-norm upper bound, not a fitted error estimate. Thus the unreduced source has the auditable decomposition

$$A_{\mathrm{src}} = D + K_{\mathrm{cross}} + K_{\mathrm{smooth}} - \big(\log a + \log(2\pi) + \gamma\big)I - \sum_{n=2,3,4} \frac{\Lambda(n)}{\sqrt{n}}\,\mathcal{A}_n, \tag{25}$$

where $\mathcal{A}_n$ is the identity-block adjacency matrix of the printed n-edge list. No quadrature is used in (25).

Reflection sends e_{rj} to $(-1)^j e_{12-r,j}$. Hence the parity isometries $U_\pm : \mathbb{R}^{78} \to \mathbb{R}^{156}$ have paired columns

$$2^{-1/2}\big(e_{rj} \pm (-1)^j e_{12-r,j}\big), \qquad 0 \le r < 6, \tag{26}$$

together with the even, respectively odd, modes of the central interval. The implementation checks $U_\pm^T U_\pm = I$, $U_+^T U_- = 0$, and reconstructs the unreduced spectrum before exporting $U_\pm^T A_{\mathrm{src}} U_\pm$.

A.2 Complement rows and positive Grams

For a target interval t and complement degree $q \ge 12$, let $v_{tq} \in \mathbb{R}^{156}$ collect the coefficients of the exact second-Green map from all source modes into that target mode. Its self-block entry is

$$(v_{tq})_{tj} = \mathbf{1}_{q+j \text{ even}} \frac{\sqrt{(2q+1)(2j+1)}}{(q-j)(q+j+1)}, \tag{27}$$

and the adjacent and separated entries are the corresponding exact Legendre–Green integrals, with the orientation factor $(-1)^{q+j}$ when the source lies to the left. The finite band Gram is therefore, before parity reduction,

$$G^J = \sum_{t=0}^{12} \sum_{q\in J} v_{tq} v_{tq}^T \succeq 0. \tag{28}$$

All cross terms between different source intervals are retained inside each outer product. Formula (28) is evaluated independently for each singleton band $J = [q, q+1)$, $12 \le q < 24$.

The endpoint-flux Gram retains rows $p_t^{\pm}$ at every interval endpoint and uses the exact weights

$$\sum_{q=N}^{M-1} \frac{2q+1}{2q^2(q+1)^2} (p_t^+ - (-1)^q p_t^-)(p_t^+ - (-1)^q p_t^-)^T, \tag{29}$$

plus the positive M^{-2} remainder. We now define the coefficient appearing in the adjacent-singular row without reference to software. On a source interval of length ℓ_r, write

$$f_j^{(r)}(u) = \sqrt{\frac{2j+1}{\ell_r}} P_j(2u/\ell_r - 1), \qquad \widetilde{f}_j^{(r)}(u) = f_j^{(r)}(-u), \tag{30}$$

$$g_k^{(t)}(u) = \sqrt{\frac{2k+1}{\ell_t}} P_k(1 - 2u/\ell_t), \qquad 0 \le u \le \ell_t. \tag{31}$$

Set

$$R_j^{t\leftarrow r}(u) := -\frac{1}{2}\left[(\ell_t - 2u)(\widetilde{f}_j^{(r)})'(u) + u(\ell_t - u)(\widetilde{f}_j^{(r)})''(u)\right], \qquad C_{t\leftarrow r}^{kj} := \int_0^{\ell_t} g_k^{(t)}(u) R_j^{t\leftarrow r}(u)\, du. \tag{32}$$

All functions in (32) are polynomials, so the generator expands them in monomials and evaluates the integral exactly as $\sum_{p,q} g_{kp} R_{jq} \ell_t^{p+q+1}/(p+q+1)$ in Arb. The adjacent-singular row is then

$$s_{tq,j} = -\sum_{k<12} \frac{\sqrt{(2q+1)(2k+1)}}{q(q+1) - k(k+1)} \frac{C_{kj}^{t\leftarrow r}}{q(q+1)}, \tag{33}$$

summed over both neighbours $r = t \pm 1$ before squaring. Finally, the retained self-regularized row is

$$r_{qj} = \mathbf{1}_{q-j\ \text{even}} \frac{\sqrt{(2q+1)(2j+1)}\, j(j+1)}{[q(q+1) - j(j+1)]q(q+1)}. \tag{34}$$

Analytic remainders of (33) and (34) enter as positive diagonal Grams; the remaining non-directional map is bounded by the smaller of its Arb spectral estimate and the Schur row–column norm.

Table 2: Normative source-to-Gram map. Every listed object is checked for shape, finiteness, nonnegative radii, and its registered metadata.

object	mathematical content	generator / exported field
finite source	(25), then (26)	`arb_third_window_source.build_arb_third_window_source`; `source_even/odd_*`
degree band	complete rows (28), including smooth map	`arb_third_window_near_tail_gram.build_arb_third_window_near_tail_gram`; `band_i_even/odd_*`
endpoint flux	(29) and positive remainder	`arb_third_window_flux_gram.build_arb_third_window_flux_gram`; `flux_even/odd_*`
adjacent singular	both neighbours combined before the Gram	`arb_third_window_singular_gram.build_arb_third_window_singular_gram`; `singular_even/odd_*`
directional self	(34) and diagonal remainder	`arb_third_window_self_gram.build_arb_third_window_self_gram`; `self_even/odd_*`
other tail	adjacent/separated analytic comparison matrix	`arb_third_window_other_tail.certify_third_window_other_tail`; `other_tail_norm`
final sign	multiband Schur, Arb congruence–Gershgorin, Lemma 5.3	`third_window_multiband_schur_certificate.certify_third_window_multiband_schur`

A.3 One-line reconstruction of the certificate

With $\eta = 0.2$, $\rho = 10^{-4}$, and ϵ_{oth} the certified other-tail norm, define

$$G_{\text{str}} = 2(G_{\text{flux}} + G_{\text{sing}}), \tag{35}$$

$$G_{\text{tail}} = (1+\rho)\big((1+\eta)G_{\text{str}} + (1+\eta^{-1})G_{\text{self}}\big) + (1+\rho^{-1})\epsilon_{\text{oth}}^2 I. \tag{36}$$

For each parity the exact matrix submitted to the interval sign test is

$$S_\pi = A_{\mathrm{src},\pi} - r_{\mathrm{sm}} I - \sum_{m=12}^{23} \frac{G_\pi^{[m,m+1)}}{d_m} - \frac{G_\pi^{[24,176)}}{d_{24}} - \frac{G_{\mathrm{tail},\pi}}{d_{176}}. \tag{37}$$

The residual band is formed as an interval subtraction $G^{[24,176)} = G^{[12,176)} - \sum_{m=12}^{23} G^{[m,m+1)}$. Thus (37) fixes every sign, denominator, and remainder used in Table 1.

For completeness, Table 3 prints the three outward endpoints inserted in Lemma 5.3: s is the certified Schur lower bound, d the complement lower bound, and b the coupling-norm upper bound. Substitution into (20) reproduces the last column directly.

Table 3: Full-block transport constants.

sector	s (lower)	d (lower)	b (upper)	full lower bound
even	$1.5503334138073538\,10^{-14}$	0.220973215897795	3.364050436902478	$5.890068275105137\,10^{-17}$
odd	$4.368297840510665\,10^{-11}$	0.220973215897795	3.3712214851682476	$1.6529959078469627\,10^{-13}$

B Independent reconstruction audit

The release contains `independent_reference_audit.py`. It imports neither project modules nor python-flint. From the printed cut points it reconstructs all eleven prime-power edges, verifies the $78 + 78$ parity isometries, loads only the raw component balls, and independently evaluates (36)–(37) with 100-decimal mpmath arithmetic. Weyl's inequality is then applied using the maximum radius row sum. The shadow margins are

$$\lambda_{\min}(M_+) - \|R_+\|_\infty > 6.3113 \times 10^{-14}, \qquad \lambda_{\min}(M_-) - \|R_-\|_\infty > 4.3738 \times 10^{-11}.$$

This implementation is intentionally not invoked by the Arb proof and does not replace its directed-rounding guarantee. Its role is orthogonal: it makes a wrong edge list, parity convention, residual-band sign, balance factor, or denominator fail through a separately written assembly path. The corrected source replay additionally regenerates the component Grams from the explicit formula, rather than merely rereading the registered NPZ objects.

AI assistance disclosure

AI tools assisted with literature discovery, adversarial proof checking, software inspection, and manuscript preparation. The author selected the claims, reviewed the mathematical arguments and executable evidence, and is responsible for the final text and any remaining errors.

References

[1] H. Yoshida, *On Hermitian forms attached to zeta functions*, in Zeta Functions in Geometry, Adv. Stud. Pure Math. 21 (1992), 281–325.

[2] E. Bombieri, *Remarks on Weil's quadratic functional in the theory of prime numbers, I*, Rend. Lincei Mat. Appl. 11 (2000), 183–233.

[3] A. Connes and C. Consani, *Spectral triples and ζ-cycles*, Enseign. Math. 69 (2023), 93–148.

[4] A. Connes, C. Consani and H. Moscovici, *Zeta spectral triples*, arXiv:2511.22755 (2025).

[5] M. Suzuki, *Weil's quadratic form via the screw function*, arXiv:2606.09096 (2026).

[6] T. Kim, Y. Hong, M. Kim, S. Choi, J. Jang, J. Shin and M. Kim, *A numerical realization of Suzuki's Weil-quadratic-form operator: the Archimedean spectral law, its universality, and an operator form of Weil's positivity criterion*, arXiv:2607.24830 (2026).

[7] M. R. Rosenzweig and S. J. Stanfill, *On the fundamental solutions of two nonlocal parabolic equations related to logarithmic Laplacians*, arXiv:2606.04225 (2026).

[8] G. H. Golub and J. H. Welsch, *Calculation of Gauss quadrature rules*, Math. Comp. 23 (1969), 221–230.

[9] H. Fawzi, J. Saunderson and P. A. Parrilo, *Semidefinite approximations of the matrix logarithm*, Found. Comput. Math. 19 (2019), 259–296.

[10] E. V. Haynsworth, *Determination of the inertia of a partitioned Hermitian matrix*, Linear Algebra Appl. 1 (1968), 73–81.

[11] B. Simon, *A canonical decomposition for quadratic forms with applications to monotone convergence theorems*, J. Funct. Anal. 28 (1978), 377–385.

[12] T. Kato, *Perturbation Theory for Linear Operators*, Springer, 1995.